Biomedical Optics EXPRESS

Enhanced localized plasmonic detections using partially-embedded gold nanoparticles and ellipsometric measurements

Rakesh Singh Moirangthem,[1, 2, 3] Mohammad Tariq Yaseen,[1, 2, 3] Pei-Kuen Wei,[1] Ji-Yen Cheng,[1] and Yia-Chung Chang[1]*

[1]*Research Centre for Applied Sciences, Academia Sinica, Taipei, 115, Taiwan*
[2]*Department of Engineering and System Science, National Tsing Hua University, Hsinchu 300, Taiwan*
[3]*Nano Science and Technology Program, Taiwan International Graduate Program, Academia Sinica, Taipei 115, Taiwan*
yiachang@gate.sinica.edu.tw

Abstract: A cost-effective, stable and ultrasensitive localized surface plasmon resonance (LSPR) sensor based on gold nanoparticles (AuNPs) partially embedded in transparent substrate is presented. Partially embedded AuNPs were prepared by thermal annealing of gold thin films deposited on glass at a temperature close to the glass transition temperature of the substrate. Annealed samples were optically characterized by using spectroscopic ellipsometry and compare with theoretical modeling to understand the optical responses from the samples. By combining the partially-embedded AuNPs substrate with a microfluidic flow cell and dove prism in an ellipsometry setup, an ultrasensitive change in the LSPR signal can be detected. The refractive index sensitivity obtained from the phase measurement is up to 1938 degrees/RIU which is several times higher than that of synthesized colloidal gold nanoparticles. The sample is further used to investigate the interactions between primary and secondary antibodies. The bio-molecular detection limit of the LSPR signal is down to 20 pM. Our proposed sensor is label free, non-destructive, with high sensitivity, low cost, and easy to fabricate. These features make it feasible for commercialization in biomedical applications.

OCIS codes: (120.2130) Ellipsometry and polarimetry; (240.6680) Surface plasmons; (280.1415) Biological sensing and sensors; (280.4788) Optical sensing and sensors.

References and links

1. S. A. Maier, *Plasmonics: Fundamentals and Applications* (Springer, 2007).
2. A. D. McFarland and R. P. Van Duyne, "Single silver nanoparticles as real-time optical sensors with zeptomole sensitivity," Nano Lett. **3**(8), 1057–1062 (2003).
3. M. M. Miller and A. A. Lazarides, "Sensitivity of metal nanoparticle surface plasmon resonance to the dielectric environment," J. Phys. Chem. B **109**(46), 21556–21565 (2005).
4. N. Nath and A. Chilkoti, "A colorimetric gold nanoparticle sensor to interrogate biomolecular interactions in real time on a surface," Anal. Chem. **74**(3), 504–509 (2002).
5. V. G. Kravets, F. Schedin, A. V. Kabashin, and A. N. Grigorenko, "Sensitivity of collective plasmon modes of gold nanoresonators to local environment," Opt. Lett. **35**(7), 956–958 (2010).
6. J. N. Anker, W. P. Hall, O. Lyandres, N. C. Shah, J. Zhao, and R. P. Van Duyne, "Biosensing with plasmonic nanosensors," Nat. Mater. **7**(6), 442–453 (2008).
7. S. W. Lee, K. S. Lee, J. Ahn, J. J. Lee, M. G. Kim, and Y. B. Shin, "Highly sensitive biosensing using arrays of plasmonic Au nanodisks realized by nanoimprint lithography," ACS Nano **5**(2), 897–904 (2011).
8. I. H. El-Sayed, X. Huang, and M. A. El-Sayed, "Surface plasmon resonance scattering and absorption of anti-EGFR antibody conjugated gold nanoparticles in cancer diagnostics: applications in oral cancer," Nano Lett. **5**(5), 829–834 (2005).
9. T. Okamoto, I. Yamaguchi, and T. Kobayashi, "Local plasmon sensor with gold colloid monolayers deposited upon glass substrates," Opt. Lett. **25**(6), 372–374 (2000).
10. N. Nath and A. Chilkoti, "Label-free biosensing by surface plasmon resonance of nanoparticles on glass: optimization of nanoparticle size," Anal. Chem. **76**(18), 5370–5378 (2004).

#162886 - $15.00 USD Received 10 Feb 2012; revised 23 Mar 2012; accepted 4 Apr 2012; published 9 Apr 2012

11. T. A. Bendikov, A. Rabinkov, T. Karakouz, A. Vaskevich, and I. Rubinstein, "Biological sensing and interface design in gold island film based localized plasmon transducers," Anal. Chem. **80**(19), 7487–7498 (2008).
12. X. Zhang, J. Zhang, H. Wang, Y. Hao, X. Zhang, T. Wang, Y. Wang, R. Zhao, H. Zhang, and B. Yang, "Thermal-induced surface plasmon band shift of gold nanoparticle monolayer: morphology and refractive index sensitivity," Nanotechnology **21**(46), 465702 (2010).
13. G. Kalyuzhny, M. A. Schneeweiss, A. Shanzer, A. Vaskevich, and I. Rubinstein, "Differential plasmon spectroscopy as a tool for monitoring molecular binding to ultrathin gold films," J. Am. Chem. Soc. **123**(13), 3177–3178 (2001).
14. T. Karakouz, D. Holder, M. Goomanovsky, A. Vaskevich, and I. Rubinstein, "Morphology and refractive index sensitivity of gold island films," Chem. Mater. **21**(24), 5875–5885 (2009).
15. T. Karakouz, A. B. Tesler, T. A. Bendikov, A. Vaskevich, and I. Rubinstein, "Highly stable localized plasmon transducers obtained by thermal embedding of gold island films on glass," Adv. Mater. (Deerfield Beach Fla.) **20**(20), 3893–3899 (2008).
16. O. Kedem, A. B. Tesler, A. Vaskevich, and I. Rubinstein, "Sensitivity and optimization of localized surface plasmon resonance transducers," ACS Nano **5**(2), 748–760 (2011).
17. O. Kedem, A. Vaskevich, and I. Rubinstein, "Improved sensitivity of localized surface plasmon resonance transducers using reflection measurements," J. Phys. Chem. Lett. **2**(10), 1223–1226 (2011).
18. A. J. Haes and R. P. Van Duyne, "A unified view of propagating and localized surface plasmon resonance biosensors," Anal. Bioanal. Chem. **379**(7-8), 920–930 (2004).
19. L. S. Jung, C. T. Campbell, T. M. Chinowsky, M. N. Mar, and S. S. Yee, "Quantitative interpretation of the response of surface plasmon resonance sensors to adsorbed films," Langmuir **14**(19), 5636–5648 (1998).
20. R. S. Moirangthem, Y. C. Chang, S. H. Hsu, and P. K. Wei, "Surface plasmon resonance ellipsometry based sensor for studying biomolecular interaction," Biosens. Bioelectron. **25**(12), 2633–2638 (2010).
21. H. Fujiwara, *Spectroscopic Ellipsometry: Principles and Applications* (John Wiley & Sons, 2007).
22. A. Serrano, O. Rodríguez de la Fuente, and M. A. García, "Extended and localized surface plasmons in annealed Au films on glass substrates," J. Appl. Phys. **108**(7), 074303 (2010).
23. D. Aspnes, "Optical properties of thin films," Thin Solid Films **89**(3), 249–262 (1982).
24. R. W. Cohen, G. D. Cody, M. D. Coutts, and B. Abeles, "Optical properties of granular silver and gold films," Phys. Rev. B **8**(8), 3689–3701 (1973).
25. J. M. Lamarre, Z. Yu, C. Harkati, S. Roorda, and L. Martinu, "Optical and microstructural properties of nanocomposite Au/SiO2 films containing particles deformed by heavy ion irradiation," Thin Solid Films **479**(1-2), 232–237 (2005).
26. D. Aspnes, "Plasmonics and effective-medium theories," Thin Solid Films **519**(9), 2571–2574 (2011).
27. T. W. H. Oates, H. Wormeester, and H. Arwin, "Characterization of plasmonic effects in thin films and metamaterials using spectroscopic ellipsometry," Prog. Surf. Sci. **86**(11-12), 328–376 (2011).
28. M. Lončarić, J. Sancho-Parramon, and H. Zorc, "Optical properties of gold island films - a spectroscopic ellipsometry study," Thin Solid Films **519**(9), 2946–2950 (2011).
29. I. R. Hooper and J. R. Sambles, "Sensing using differential surface plasmon ellipsometry," J. Appl. Phys. **96**(5), 3004–3011 (2004).
30. R. S. Moirangthem, Y. C. Chang, and P. K. Wei, "Investigation of surface plasmon biosensing using gold nanoparticles enhanced ellipsometry," Opt. Lett. **36**(5), 775–777 (2011).
31. S. G. Nelson, K. S. Johnston, and S. S. Yee, "High sensitivity surface plasmon resonance sensor based on phase detection," Sens. Actuators B Chem. **35**(1-3), 187–191 (1996).
32. K. M. Mayer and J. H. Hafner, "Localized surface plasmon resonance sensors," Chem. Rev. **111**(6), 3828–3857 (2011).
33. D. Gerion and G. J. Day, "Localized surface plasmon resonance for bioprocess development, monitoring, and validation," BioProcess Int. **9**, 70–75 (2011).
34. G. Frens, "Controlled nucleation for the regulation of the particle size in monodisperse gold suspensions," Nat. Phys. Sci. **241**, 20–22 (1973).

1. Introduction

The optical response of metallic nanoparticles with size of few tens of nanometers can lead to localized surface plasmon resonance (LSPR) resulting from the coupling of collective excitation of the conduction electrons with the incident light. The frequency at which the maximal response due to the charge oscillation in the metallic nanoparticle occurs is defined as the localized surface plasmon resonance (LSPR) frequency [1]. The position and intensity of LSPR frequency is sensitive to the size, shape and inter-particle distance, and refractive indices of the surrounding materials [2,3]. This particular property has fostered applications in bio-medical sensors, which detect local refractive index changes of the medium near the nanoparticle surface as a consequence of bio-molecular binding. Plasmonic biosensor based on gold nanoparticles with different shape prepared through various techniques such as colloidal lithography, electron beam lithography, nanosphere lithography and nano-imprint lithography etc., have been studied for decades [4–7]. Among these techniques, colloidal synthesized metal nanoparticles are more promising in the areas of biological sensing and

#162886 - $15.00 USD Received 10 Feb 2012; revised 23 Mar 2012; accepted 4 Apr 2012; published 9 Apr 2012

diagnostic applications due to their ease of preparation, cost effectiveness and readiness for bio-conjugation, etc. [8]. More precisely, chip based LSPR biosensor has been demonstrated by various groups for studying bio-molecular interaction in which the gold nanoparticles (AuNPs) prepared through colloidal synthesis were immobilized on the functionalized glass substrate [9,10]. However, it has to be noted that samples prepared via chemical modification suffer a major obstacle of instability upon exposure to various solvents i.e., the AuNPs may be washed away with the solvent [11]. The poor attachment of the AuNPs on the glass can be improved through high-temperature thermal annealing of the AuNPs film [12]. However, the preparations of the high quality sample as well as surface modifications of glass surface are critical issues which may require special expertise. Hence a simple, cheap and effective technique to prepare AuNPs on glass surface is needed to overcome this issue. Rubinstein et.al, reported a highly stable localized plasmon transducers based on the gold films embedded in glass substrate and their surface morphologies have been discussed in details through Atomic Force Microscope (AFM) [13–15]. So far, the achieved refractive index (RI) sensitivity on this embedded metal nanostructure does not exceed 100-300 nm/RIU in spectral interrogation schemes [16,17] and has 10 times smaller probe depth [6,17,18], as compared to the conventional SPR system making them applicable for only a very limited number of biological species. It has to be noted that the refractive index (RI) sensitivity is a key factor that determines the detection limit of the LSPR sensor [19]. Thus, there is a need for an improvement in the sensitivity for this LSPR sensor. In this study, we present a systematic investigation of highly sensitive sensors made of partially embedded gold nanoparticles prepared via thermal annealing of Au thin films on glass substrates. Quantitative studies on the annealed Au films were studied via ellipsometry measurements with efficient theoretical modeling. To perform the experiments in the aqueous solutions, the prepared samples were fixed on the home-made micro-fluidic flow cell and placed on top of a dove prism which was integrated with the spectroscopic ellipsometry setup [20]. The optimal thickness of the annealed gold films having highest RI sensitivity was determined using our prism-assisted spectroscopic ellipsometry. Comparisons on the RI sensitivity under ellipsometric phase interrogation scheme were also made with colloidal AuNPs of different sizes immobilized on glass substrate. It shows that embedded AuNPs result in significant improvement in the RI sensitivity. Numerical simulations were also conducted to verify the enhancement in the sensitivity of the proposed plasmonic sensor. Furthermore, the possible application of proposed optical tool with this highly sensitive biochip in biomedical application is demonstrated by monitoring the interactions between primary (anti-EGFR) and secondary antibodies in dynamic mode.

2. Experimental section

2.1. Fabrication of embedded gold nanoparticles

The glass slides (Gold Seal, USA) were first cleaned by piranha solution (70% H_2SO_4: 30% H_2O_2) followed by rinsing with ultra-pure water (Milli-Q Element, Millipore). It was subsequently cleaned in an ultrasound bath with acetone and isopropyl solution for 20 minutes each and finally rinsed with water. The cleaned glass slides were dried in oven prior to metal deposition. The gold (Au) films with thickness of 4, 5, 6, 8 and 10 nm were deposited using e-gun evaporator (AST, Taiwan) at a deposition rate of 0.1 Å/sec, the deposited thickness was further confirmed with ellipsometry measurement in the spectral range of 300 to 1000 nm. Then, the as-deposited samples were put inside a furnace (Lindberg/Blue) for annealing in air at 550°C which is close to the glass transition temperature of the glass substrate. The annealing process was divided into three steps: (1) during the initial stage of 3 hrs., temperature was set to gradually increase from room temperature to target temperature, (2) constant heating at target temperature for 3 hrs. and (3) cooling for another 8 hrs. from target temperature to room temperature. When the Au film is annealed at a temperature close to the glass transition (GT) temperature (550°C for our case), it leads to the formation of partially embedded AuNPs.

#162886 - $15.00 USD Received 10 Feb 2012; revised 23 Mar 2012; accepted 4 Apr 2012; published 9 Apr 2012

2.2. Synthesis of colloidal gold nanoparticles and sample preparation

5mM concentration of Gold(III) chloride trihydrate ([$HAuCl_4.3H_2O$], Sigma Aldrich) and 38.8mM concentration of sodium citrate tribasic dehydrate (Sigma Aldrich) were prepared in ultrapure water (Millipore) as stock solutions. Various AuNPs with absorption peak at 519, 527, 537, 554 nm were prepared by diluting 6% (v/v %) of the stock solution of H[AuCl4] in ultra-pure water which was taken in double-neck conical flask mounted with water reflux tube. The solution was maintained at 130°C by placing in silicon oil bath and stirred with a magnetic stirrer at 500 rpm for 30 minutes. Different concentrations of sodium citrate were added drop-by-drop into the solution with stirring and heating and waited for 12 minutes. The color of the H[$AuCl_4$] solution changed from black to reddish, indicating the formation of AuNPs. The prepared colloidal AuNPs solution was cooled down to room temperature and stored in refrigerator until use. For the sample preparation, the glass substrates pre-cleaned with piranha solution were immersed in 10% (v/v) solution of (3-aminopropyl) triethoxysaline (APTES, Sigma Aldrich) in anhydrous ethanol for 20 minutes, rinsed for five times in ethanol with sonication and dried at 120°C for 2 hours. The AuNPs were poured on the silanized glass surface for 24 hours in humid environment to avoid the evaporation of the colloidal AuNPs solution from the surface and to ensure complete coverage to minimize variations in the sensitivity between different batches of the nanoparticles immobilized on the substrate.

2.3. Protein immobilization and measurements

For biological experiments the primary antibody e.g. mouse anti-human epidermal growth factor receptor (anti-EGFR) [BD Pharmingen, USA] and goat anti-mouse IgG (secondary antibody) [Chemicon, USA] were diluted in 1X phosphate buffer saline (PBS, pH-7.4) [Sigma Aldrich] solutions with concentration of 10 and 50 μg/ml, respectively. In the experiment, PBS solution was first injected into the microchip and the measured signal was set as the baseline signal. Then, anti-EGFR was introduced onto the embedded AuNPs surface and incubated for 90 minutes under static condition in order to capture sufficient coverage of the biomolecules. The sample was rinsed with PBS solution to remove unbound primary antibodies. Finally, secondary antibody (IgG) was injected onto the surface of the biochip and kept under static condition for another 90 minutes, followed by rinsing with PBS solution to wash away the unbound antibodies. The dynamic measurements were performed by using a prism-assisted ellipsometry, which measured the changes of LSPR signals in both amplitudes and phases.

3. Results and discussion

3.1. Theoretical analysis

Ellipsometry refers to a self-referencing optical characterization tool. It measures the polarization states of the electric field before and after reflection from the sample. The simultaneous measurement of the ellipsometry parameters, Ψ and Δ (the magnitude and phase of the ratio of p- and s-polarized reflectivities), provides rich information about the sample under investigation. In the reflection mode, Ψ and Δ are defined by [21]

$$\tan\Psi = \left|\frac{R_p}{R_s}\right| \text{and } \Delta = \delta_p - \delta_s \quad (1)$$

where R_p and R_s are the complex-valued reflection coefficients for the polarization parallel (p) and perpendicular (s) to the plane of incidence; δ_p and δ_s are the phases of R_p and R_s. For ellipsometry in the prism-assisted configuration, the plane of incidence needs to be redefined. There is also imperfect transmission taking place at the interfaces between air and the prism at an oblique angle, which needs to be considered. Thus, the experimental results obtained by prism-assisted ellipsometry were transformed by using Eq. (2) of Ref [20]. in order to analyze the data with the J. A. Woolam ellipsometer-equipped software (WVASE32).

#162886 - $15.00 USD Received 10 Feb 2012; revised 23 Mar 2012; accepted 4 Apr 2012; published 9 Apr 2012

3.2. Analysis of the film with partially embedded gold nanoparticles

Gold thin films deposited over substrates with poor adhesion exhibit substantial modifications when annealed in air at high temperature, which leads to the formation of nanoparticles agglomeration in order to reduce the surface energy. The formation of hillock structure is due to the relaxation of the thermal stress during the course of annealing process where the metal and the substrate have different thermal expansion coefficients [22]. For Au deposited on glass substrate, the annealing at the vicinity of the glass transition (Tg)-temperature leads to the formation of partially embedded AuNPs in glass substrate, thereby achieving highly stable Au nanostructures without any adhesive layer. This is evidenced by the presence of an LSPR peak in the absorption spectra (see Fig. 1). Figure 1(a) shows the absorption spectra of the annealed gold films with various thicknesses and the inset shows a picture of prepared sample as well as a plot of absorption peak position versus film thickness. The increase of wavelength of the LSPR absorption peak indicates that the particle size is increased with the thickness of gold film. Figure 1(b) illustrates the fabrication process for partially embedded AuNPs schematically, and Fig. 1(c) shows the SEM image of a 5nm thick Au film after annealing at 550°C, where the formation of embedded AuNPs in glass substrate can be seen clearly. The morphology changes due to annealing at different temperatures with different thickness of Au films have been discussed elsewhere [15]. Such thermally annealed samples have non-uniform size distributions; however, more than 70% show similar sizes within a range of ± 10 nm. The SEM image shown in Fig. 1(c) reveals a size distribution in the range of 70-80nm. The sizes of AuNPs are larger as the thickness of the gold film increases. The corresponding absorption peaks are red shifted [see Fig. 1(a)]. In order to design highly sensitive label-free biosensing device based on our proposed plasmonic nanostructures, systematic investigations

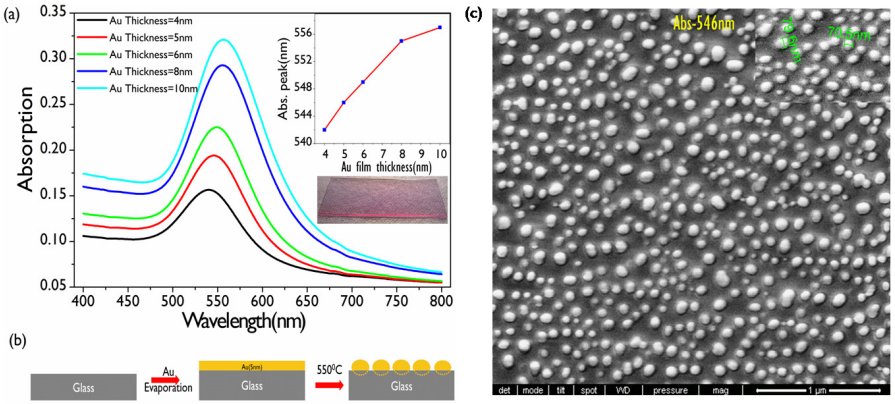

Fig. 1. (a) Absorption spectra of the thermally annealed Au film with different thickness [inset figures show a picture of prepared sample as well as a plot of absorption peak position versus film thickness]. (b) Schematic diagram showing sample fabrication process. (c) SEM image of 5nm thick gold film after annealing, which has an absorption peak at 546nm. [The measured sizes of the gold nano islands are labeled in the inset].

on the optical properties of these embedded nanoparticles are needed. A quantitative study on partially embedded AuNPs in glass substrate by using spectroscopic ellipsometry will be discussed next. The ellipsometric signals Ψ and Δ defined by Eq. (1) as functions of wavelength were obtained at various angles of incidence. Various theoretical approaches have been proposed to calculate the optical response from spherical as well as non-spherical metal nanoparticles, including simple effective medium approximation (EMA) theory and sophisticated theory using multipole expansion method such as GRANFILM. In our simulation, we adopted simple EMA (Maxwell-Garnett theory, MGT) with depolarization factor (DF). The incorporation of the depolarization factor in the MGT allows us to consider the effect of the non-spherical shapes to some extent, whereas the bare MGT (assuming spherical particles) does not work well [23–26]. Thus in our theoretical model, we divided the

#162886 - $15.00 USD Received 10 Feb 2012; revised 23 Mar 2012; accepted 4 Apr 2012; published 9 Apr 2012

film with embedded gold nano islands into two EMA layers and parts of gold nanostructures in each EMA layer are treated as ellipsoidal nanostructures. However, the strength of plasmonic resonances related to the aspect ratio (length/width) of an ellipsoidal nanostructure was not consider in our calculation, which is beyond the scope of our investigation. The effective plasmonic resonance for the whole system can be obtained by considering the combined effect of all EMA layers. A Detail theoretical analysis on such problem can be found in the recent review article by Oates et.al [27]. With this simple assumption, we are able to fit the experimental data very well over the measured spectral range from 300 to 1000nm. We used the WVASE32 software to fit and extract the dielectric constants of EMA layers for both partially embedded and exposed portions. Figures 2(a)–2(c) show the ellipsometry data together with best-fit simulation results for the 5nm-thick annealed Au film. A schematic plot of the model used in the fitting of the experimental data is illustrated in Fig. 2(d). The extracted dielectric constants of EMA layer for embedded AuNPs partially exposed to air (1st EMA) and those for AuNPs embedded in glass (2nd EMA) are shown in Fig. 2(e) and 2(f), respectively. The model generated reflectance spectrum for TM mode fits the measured data fairly well [see Fig. 2(c)]. Similar measurements and theoretical simulations were done on samples with different thickness. Detailed fitting results for the volume fractions of AuNPs in EMA layers, depolarization factor, and effective layer thicknesses are provided in Table 1. As it can be seen from the Fig. 2, that the model generated spectra fit the data very well over the measured spectral range at multiple angles of incidence, which indicates the adequacy of our model as compared to more sophisticated models [28]. Thus, we have illustrated that the spectroscopic ellipsometry can serve as a convenient optical metrology tool for checking the formation of partially embedded AuNPs.

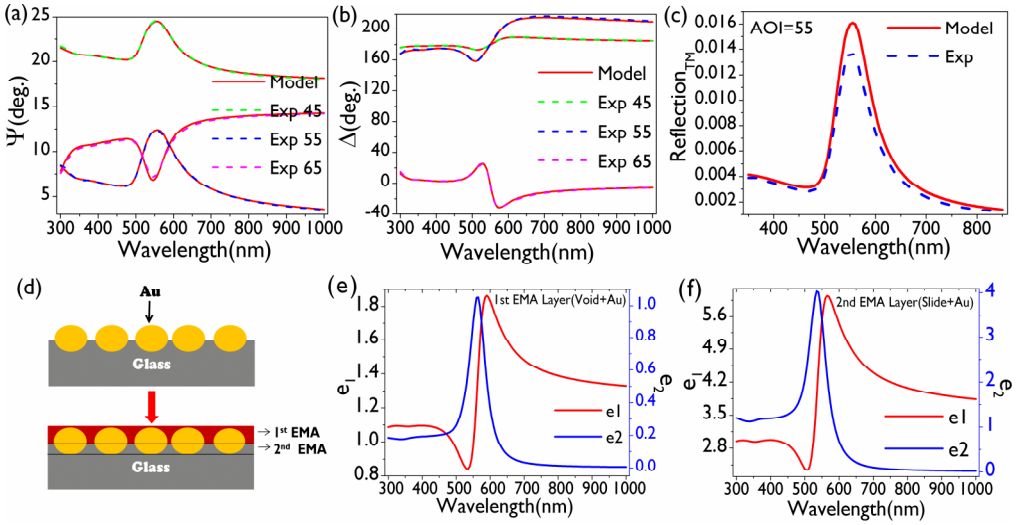

Fig. 2. Spectral response of the ellipsometric parameters (a) Ψ, (b) Δ, and (c) TM-mode reflectance spectrum for 5nm thick annealed Au film shown together with the model generated spectrum. (d) Schematic plot of the model used to fit the experimental data. (e) & (f) Dielectric constants of the AuNPs exposed to air and embedded in glass substrate.

#162886 - $15.00 USD Received 10 Feb 2012; revised 23 Mar 2012; accepted 4 Apr 2012; published 9 Apr 2012

Table 1. Ellipsometry fitting parameters of the different thickness of annealed gold thin films where $\%f_{Void}$, $\%f_{Slide}$, $\%f_{Gold}$ represent the fractional volume ration of air, glass and gold in corresponding effective medium approximation (EMA) layers.

Au Film Thickness (nm)	Calculated EMA Layers Thickness (nm)		$\%f_{Void}$	$\%f_{Slide}$	$\%f_{Gold}$	DF	MSE
4	EMA 1	6.60	95.84		4.16	0.118	2.232
	EMA 2	9.04		81.19	18.81	0.370	
5	EMA 1	7.69	96.89		3.11	0.119	2.148
	EMA 2	11.56		83.05	16.94	0.351	
6	EMA 1	4.76	94.33		5.67	0.106	2.743
	EMA 2	13.42		79.02	20.98	0.353	
8	EMA 1	2.45	96.07		3.93	0.086	2.361
	EMA 2	17.29		78.32	21.68	0.317	
10	EMA 1	2.04	96.45		3.56	0.082	4.266
	EMA 2	21.52		78.39	21.61	0.310	

3.3. Behaviours of ellipsometry signals with Au film thickness

The behaviors of the ellipsometry signals with different Au film thickness were investigated using our prism assisted ellipsometry. For these experiments, the samples were fixed on a micro-fluidic flow cell and then mounted on the top of a dove prism [see inset of Fig. 3(a)]. The measured spectroscopic ellipsometry signals (Ψ, Δ) defined by Eq. (1) for different thicknesses of annealed Au films are shown in Fig. 3(a) and 3(b). It can be seen from Fig. 3(a). that the LSPR mode appearing as a peak in the Ψ spectra is very significant for Au films with thickness less than 6nm and slowly disappear as the film thickness increases. On the other hand, the SPR mode appears as a dip in the spectrum, which becomes more prominent as film thickness increases, thereby showing a transition from LSPR to SPR mode. In addition to the experimental observation, the transition from LSPR to SPR response with increasing film thickness can be further validated by observing the behavior of ε_1, the real part of the dielectric function obtained from the above EMA analysis. Figures 3(e) and 3(f) show the extracted dielectric constants of the EMA1 layer containing AuNPs. It was found that the film with thickness of 10nm after annealing starts to have negative value in ε_1 [see Fig. 3(e)] which would give rise to the SPR response, thereby showing a prominent dip in the measured Ψ spectrum. For film thickness at 6 and 8nm, we have a slightly positive value in ε_1. However, the measured spectra shows both peak and dip, which indicates a transition state from LSPR to SPR. For annealed Au film less than 5nm thick, the small content of the gold NPs means small electron density, resulting in a positive ε_1 value for EMA layer, and thus no SPR. Instead, we obtain the LSPR response as indicated by a prominent peak in the Ψ spectra [see Fig. 3(a)]. Based on our theoretical model the extracted ε_1 and ε_2 could explain the experimental finding fairly well, but to have a full understanding of the effect of detailed structures on the optical response near the plasmon resonance would require a more sophisticated theory. The LSPR peak in the spectrum corresponds to a position where the ratio of reflection amplitude between p- to s-polarization is a maximum whereas the SPR dip in the spectrum corresponds to a position where the ratio of reflection amplitude between p- to s-polarization is a minimum [see Eq. (1)]. The ellipsometry phase signal (Δ) shows a fast increase near the LSPR resonance and a fast decrease near the SPR resonance as the thicknessof the gold film increases. For very sharp resonances, the change of phase near the resonance is expected to approach 180°. However, the phase shifts for our Δ spectra are less than 180° due to the broadening of the resonance peaks. The phase signals showing positive slope for film thickness ≤ 5nm and negative slope for film thickness 6 and 8nm are due to interplay between LSPR and SPR. For films with thickness ≥10nm, the negative slope in the phase information is attributed to the SPR response. Theoretical calculations were also conducted to confirm the experimental results. Five-layer model [prism (ambient) /glass /EMA2 /EMA1 /water] was used to calculate the ellipsometry spectra and the calculated results are shown in Fig. 3(c) and 3(d). Here, the EMA1 layer is mixture of water and AuNPs and the EMA2 layer is a mixture of glass and AuNPs. The best-fit parameters for the volume

#162886 - $15.00 USD Received 10 Feb 2012; revised 23 Mar 2012; accepted 4 Apr 2012; published 9 Apr 2012

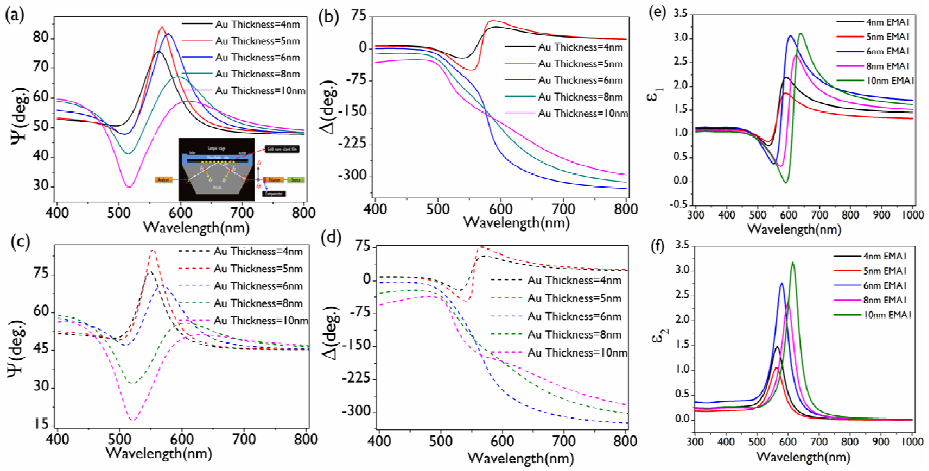

Fig. 3. Spectroscopic ellipsometric signals (a) Ψ, (b) Δ, measured under TIR mode (inset figure) for different thickness annealed Au film when expose to the water.(c) and (d) shows the calculated data using EMA.(e) and (f) shows the extracted dielectric constants of the AuNP in the EMA1 layer.

fraction of Au in EMA layers and effective thickness for various samples considered are listed in Table 1. As it can be seen from Fig. 3, the calculated ellipsometry spectra show very good agreement with experimental results, which confirms the validity of the effective-medium theory adopted here. It is further noticed that for Au films with thickness < 6nm, the ellipsometric phase (Δ) signal changes more rapidly near the LSPR resonance than the amplitude (Ψ) signal [29]. Therefore, we adopt the ellipsometry phase information as the sensing signal to check the sensitivity of the proposed plasmonic biochip.

3.4. Bulk sensitivity for annealed Au films on glass substrate

We use various aqueous solutions with different refractive indices to change the environmental conditions of AuNPs. The ellipsometry signals (Ψ,Δ) of AuNPs in solutions with different refractive indices were recorded. The measured spectral responses of ellipsometry signals for 5nm thick annealed Au film are shown in Fig. 4(a) and 4(b). The change in ellipsometry phase signals Δ at wavelength of 575nm is linear with respect to the change in refractive index (RI) [see Fig. 4(c)]. The calculated RI sensitivity obtained from the absolute value of shift in Δ for the 5nm-thick annealed Au film is 1938 ± 65 degrees/RIU. The measurements were repeated over three samples to check the variation in the sensor performance for a given thickness, and values are given in Fig. 4(c). If the phase measurement accuracy (σ_Δ) in a scheme with a fixed angle of incidence is 0.001° [30,31], the calculated RI resolution defined by $\sigma_{RI} = (\delta n / \delta\Delta)\sigma_\Delta$ [31] is about 5.16 × 10^{-7} RIU, which gives the highest refractive index sensitivity for LSPR based sensor so far reported [32,33], and is comparable to a commercial SPR machine with high precision angular resolution [for example, SPR-Navi (BioNavis Ltd., Finland)]. The dynamic range of the bulk sensitivity was chosen in a smaller range which may correspond to the change in the local refractive index upon the binding of the biomolecules on the surface of the metal nanostructure. Similar measurements were done for other thickness of annealed gold film.

#162886 - $15.00 USD Received 10 Feb 2012; revised 23 Mar 2012; accepted 4 Apr 2012; published 9 Apr 2012

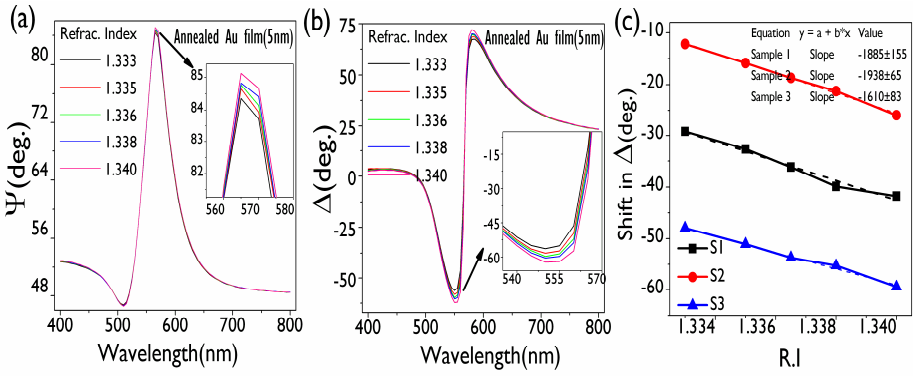

Fig. 4. Bulk sensitivity response of 5nm thick annealed Au film exposed to glycerol-water mixtures with various refractive indices by measuring the ellipsometric signals (a) Ψ, and (b) Δ. (c) Shows the change in Δ versus the change in refractive index (δn) of the surrounding aqueous medium measured at wavelength of 575nm.

3.5. Bulk sensitivity for chemically synthesis AuNPs immobilized on glass substrate

Colloidal gold nanoparticles (AuNPs) were prepared by sodium citrate reduction of chloroauric acid (H[$AuCl_4$]) solution as reported earlier with slight modification of the protocol [34]. Figure 5(a) shows the absorption spectra of the prepared colloidal AuNPs dispersed in ultrapure water measured with a UV-Visible spectrometer (Jasco, UK). The sizes of the prepared AuNPs were confirmed with scanning electron microscope (SEM, FEI Nova), giving average sizes of 13, 45, 66, and 96 nm, respectively as shown in Fig. 5(b)–5(e). Similar optical measurements were also performed for chemically synthesized AuNPs immobilized on the glass surface by exposing them to solutions of different refractive indices. Figure 6(a) and 6(b) show the ellipsometry signals (Ψ, Δ) as functions of wavelength for 45nm AuNPs immobilized on glass substrate and immersed in solutions of different refractive indices.

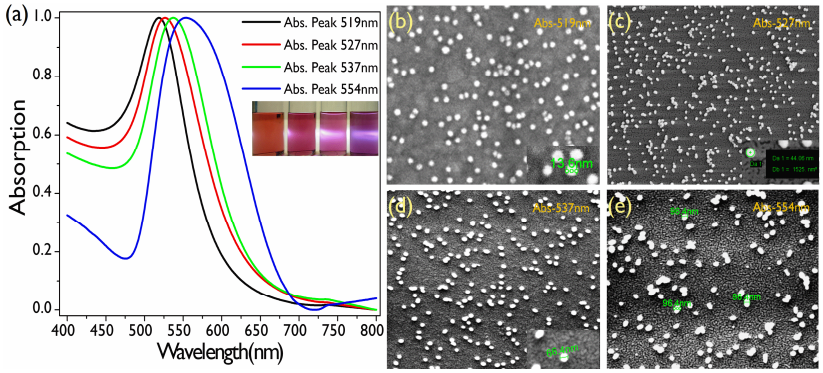

Fig. 5. (a) The absorption spectra of the colloidal gold nanoparticles in water having different sizes [Inset figure is a photograph of the prepared solutions]. SEM images of colloidal gold nanoparticle of various sizes on substrate with average sizes of (b) 13nm, (c) 45nm, (d) 66nm, and (e) 96nm.

The bulk sensitivity of the AuNPs sensor was determined from the phase signal change at a wavelength 575nm, where it gives maximum response to changes in the surrounding medium. The calculated sensitivities obtained from the slope for three different samples with similar size of AuNPs (~45nm) are shown in Fig. 6(c). The absolute value of highest sensitivity obtained from the phase signal measurement is 837 ± 87 degrees/RIU and the obtained refractive index resolution is about 1.19×10^{-6} RIU by adopting a phase measurement accuracy of 0.001°. Figure 6(d) shows the dynamic response measured at the wavelength (575nm) near LSPR with varying refractive index (δn) of the surrounding

#162886 - $15.00 USD Received 10 Feb 2012; revised 23 Mar 2012; accepted 4 Apr 2012; published 9 Apr 2012

medium. Similarly, the bulk sensitivities of various sizes of AuNPs were also calculated. The comparisons of RI sensitivities of the thermally annealed Au films and those of AuNPs of various sizes are given in Fig. 7.

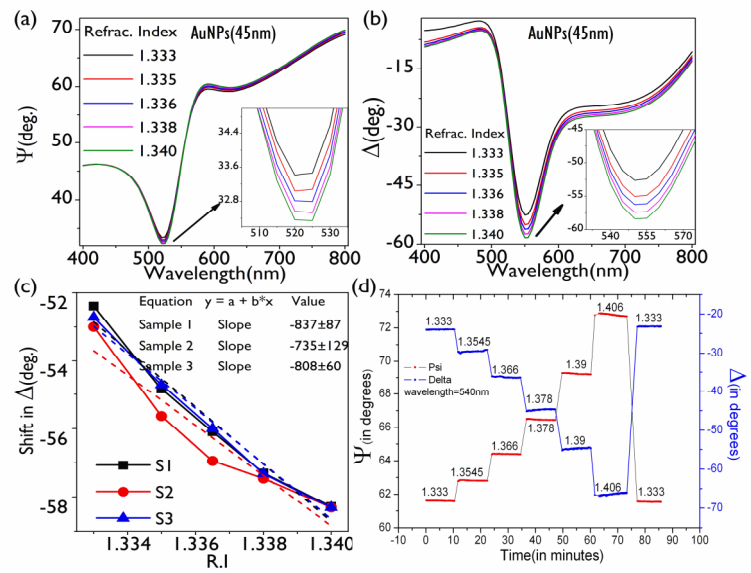

Fig. 6. Spectral response of the ellipsometric parameters for (a) Ψ, and (b) Δ for glycerol-water mixtures with various refractive indices, changes of phase signal, Δ (c) and the dynamic response (d) measured at fixed wavelength (575nm) with varying refractive index (δn) of glycerol-water mixtures. Measurements are done on the 45nm AuNPs film.

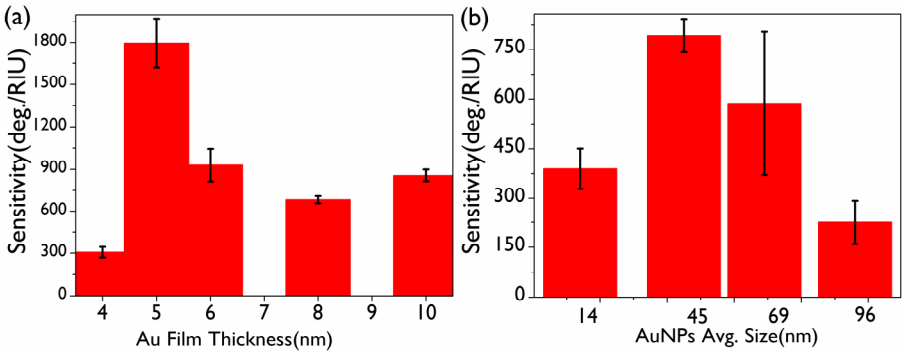

Fig. 7. Comparison of bulk sensitivity for (a) thermally annealed Au film with different thickness of 4, 5, 6, 8,10nm and (b) AuNPs of different sizes 13, 45, 66, 96nm based in the ellipsometric phase signals, Δ.

It is clear that the sample with average AuNPs diameter of 45nm shows highest sensitivity while the sample with average AuNPs diameter of 96nm shows the lowest sensitivity [see Fig. 7(b)]. This average size of AuNPs showing highest sensitivity is similar to that reported previously [10]. In Ref. 10, it was shown that AuNPs with size ranging from 35nm to 45nm in diameter exhibit maximum sensitivity to the change of the bulk refractive index. For the thermally annealed Au film, the film thickness with 5nm shows the highest sensitivity among all the thicknesses used for this study. From this study, it is found that partially embedded AuNPs in glass substrate has a much higher RI sensitivity than that of the AuNPs immobilized on the glass substrate. In order to explain the enhancement in the sensitivity for partially embedded AuNPs, we examine the electric field distributions under the illumination of TM polarized light. Numerical simulations based on Finite Differential Time Domain (FDTD)

#162886 - $15.00 USD Received 10 Feb 2012; revised 23 Mar 2012; accepted 4 Apr 2012; published 9 Apr 2012

method were performed for both cases by using the commercial software Rsoft. Figure 8(a) and 8(b) show the FDTD simulations for the total electric field intensity in the x-z plane. Based on 3D FDTD simulation for partially-embedded and fully-exposed gold nanoparticles with diameter of 20nm on a glass substrate under oblique-incidence (at 45 degree) illumination of light, it was found that the maximum intensity of the total electric field for the gold nanoparticle partially embedded inside the glass is much stronger than the one completely exposed in the air as seen in Fig. 8(c). In the simulation, the electric fields were calculated at the wavelength corresponding to maximum power absorption in both cases which was numerically determined. The reason for the stronger electric field for the partially embedded AuNP is due to the higher surrounding dielectric constant, which provides a larger optical contrast when compared with the negative real part of the dielectric constant of Au below its plasmon frequency. Since the nanoparticle is partially embedded in the glass, a portion of nanoparticle sees a surrounding medium with a higher dielectric constant (of glass) whereas the remaining portion sees the dielectric constant of the surrounding air. Hence, the effective surrounding dielectric constant for the partially embedded AuNP is higher than that of the nanoparticles completely exposed to the air. The stronger electric field of the partially embedded AuNPs implies higher sensitivity to small changes in refractive index of the surrounding medium.

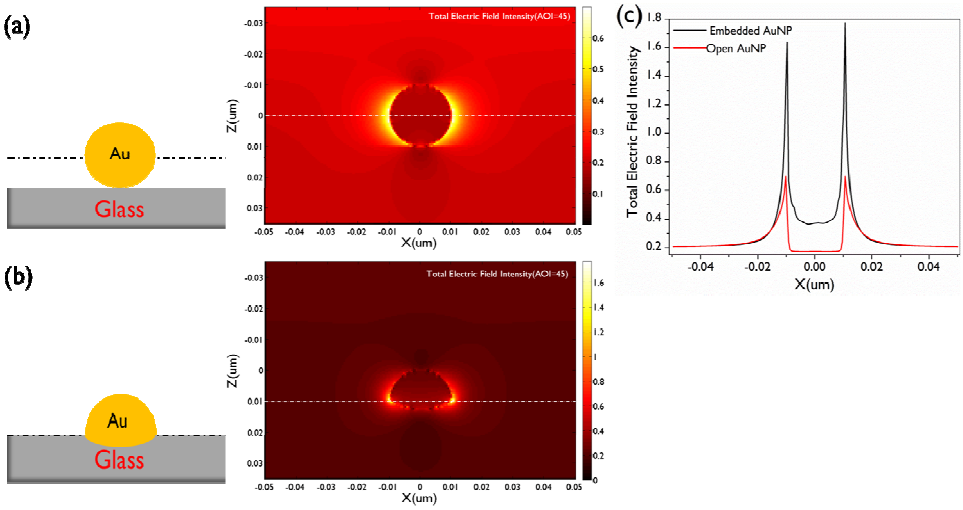

Fig. 8. A schematic plot and simulated total electric field intensity distribution maps for (a) Au nanoparticles sitting on glass which is completely exposed to the air. (b) Partially embedded Au nanoparticles in glass in the x-z plane. (c) Plot of the intensity of the electric field versus x-axis at diameter (dashed line) of gold nanoparticle partially embedded inside the glass (black color) and one completely exposed in the air (red color) for an incident angle at 45 degrees.

Similar simulations were also done for other incident angles, including normal incidence (data not shown here) and it was found that the change of the incident angle only affects the strength of the total electric field intensity (calculated as $|E|^2 = |E_x|^2 + |E_y|^2$) for both systems, but in all cases the system with embedded gold nanoparticle always gives stronger electric field as compare to the fully exposed gold nanoparticles.

3.6. Biomolecular interaction study

In this experiment, we used thermally annealed 5nm thick Au film as an LSPR biochip to monitor the biomolecular interactions. The optical signals were recorded in dynamic mode using prism-assisted ellipsometry at wavelength of 595nm. The dynamic measurement was performed at the wavelength corresponding to the highest sensitivity of the biosensor which was obtained through the spectroscopic measurements performed on the similar sample. As a

#162886 - $15.00 USD Received 10 Feb 2012; revised 23 Mar 2012; accepted 4 Apr 2012; published 9 Apr 2012

demonstration, the interaction between mouse anti-human epidermal growth factor receptor (anti-EGFR) and goat anti-mouse IgG (secondary antibody) is presented. Figure 9(a) and 9(b) show the dynamic response of the ellipsometry signals, (Ψ,Δ) upon the capturing of anti-EGFR with concentration of 10μg/ml on the partially-embedded AuNPs surface and its subsequent interaction with the secondary antibodies. The dynamic response clearly illustrates the biomolecular binding event (more pronounced in the phase signal) on the surface as well as its interaction with other specific analytes. The addition of 50μg/ml (~0.33μM) concentration of secondary antibody gives an increment in the phase signal (Δ) of ~16 degrees [see Fig. 9(b)]. Adopting a phase measurement accuracy of about 0.001°, the bio-molecular detection limit of the proposed LSPR biosensor based on ellipsometry phase signal is about 20pM (~$5.16 \times 10^{-7} \times 0.33\mu M / 0.0083$) and this value can be further improved by utilizing linker molecules to capture anti-EGFR more efficiently.

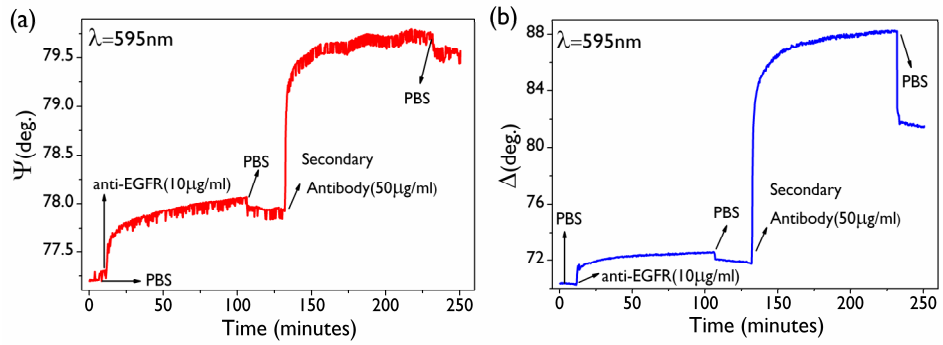

Fig. 9. (a) and (b) shows the dynamic response of the ellipsometry signals (Ψ,Δ) upon the capturing of anti-EGFR and its subsequent interaction with secondary anti-bodies.

4. Conclusions

Quantitative investigations of LSPR sensing and its application in studying biomolecular interactions based on ellipsometric phase signal are presented. Optical responses from partially-embedded AuNPs in glass substrate prepared by thermally annealed Au films show a clear transition from LSPR to SPR mode as the film thickness increases. The proposed plasmonic bio-chip was tested for bulk sensitivity response by using a prism-assisted spectroscopic ellipsometry and its sensitivity was compared to that of the gold nanoparticles immobilized on the glass substrate. It was found that partially-embedded AuNPs prepared by thermal annealing of 5nm thick gold film give the highest RI sensitivity as compared to other thicknesses. It was also found that the partially-embedded AuNPs has much higher RI sensitivity as compared to that of the AuNPs immobilized on the glass substrate. Based on the FDTD simulation, the reason for the enhancement in the sensitivity is attributed to the higher electric field localization for the partially embedded AuNPs as compared to that of the gold nanoparticle completely exposed to air. For biomedical application of this LSPR biochip, we demonstrated biomolecular interaction for primary (anti-EGFR) and secondary antibodies. The biomolecular interaction was observed in a dynamic mode, thereby providing information regarding immobilization time, interaction time, etc. Our proposed plasmonic biochip can provide a highly sensitive sensing platform, which is a promising candidate for developing a non-destructive, low cost, label free, and highly sensitive LSPR biosensor.

Acknowledgments

This work was supported by Academia Sinica, Taiwan and National Science Council of Taiwan under contracts NSC 98-2112-M-001-022-MY3.

#162886 - $15.00 USD Received 10 Feb 2012; revised 23 Mar 2012; accepted 4 Apr 2012; published 9 Apr 2012